

Accelerated Article Preview**Long-term continuous ammonia electrosynthesis**

Received: 17 July 2023

Accepted: 6 March 2024

Accelerated Article Preview

Cite this article as: Li, S. et al. Long-term continuous ammonia electrosynthesis. *Nature* <https://doi.org/10.1038/s41586-024-07276-5> (2024)

Shaofeng Li, Yuanyuan Zhou, Xianbiao Fu, Jakob B. Pedersen, Mattia Saccoccio, Suzanne Z. Andersen, Kasper Enemark-Rasmussen, Paul J. Kempen, Christian Danvad Damsgaard, Aoni Xu, Rokas Sažinas, Jon Bjarke Valbæk Mygind, Niklas H. Deissler, Jakob Kibsgaard, Peter C. K. Vesborg, Jens K. Nørskov & Ib Chorkendorff

This is a PDF file of a peer-reviewed paper that has been accepted for publication. Although unedited, the content has been subjected to preliminary formatting. Nature is providing this early version of the typeset paper as a service to our authors and readers. The text and figures will undergo copyediting and a proof review before the paper is published in its final form. Please note that during the production process errors may be discovered which could affect the content, and all legal disclaimers apply.

Long-term continuous ammonia electrosynthesis

Shaofeng Li¹†, Yuanyuan Zhou¹†, Xianbiao Fu¹, Jakob B. Pedersen¹, Mattia Saccoccio¹, Suzanne Z. Andersen¹, Kasper Enemark-Rasmussen², Paul J. Kempen³, Christian Danvad Damsgaard^{1,3}, Aoni Xu¹, Rokas Sažinas¹, Jon Bjarke Valbæk Mygind¹, Niklas H. Deissler¹, Jakob Kibsgaard¹, Peter C. K. Vesborg¹, Jens K. Nørskov^{1*}, and Ib Chorkendorff^{1*}

¹Department of Physics, Technical University of Denmark, Kongens Lyngby, Denmark

*Corresponding authors. Email: jkno@dtu.dk, ibchork@fysik.dtu.dk

²Department of Chemistry, Technical University of Denmark, Kongens Lyngby, Denmark

³National Centre for Nano Fabrication and Characterization, Technical University of Denmark, Kongens Lyngby, Denmark

†These authors contributed equally to this work

Ammonia is crucial in fertilizer and chemical industries and is seen as a carbon-free fuel¹. The ammonia electrosynthesis from nitrogen at ambient conditions offers an attractive alternative to the Haber-Bosch process^{2,3}. The lithium-mediated nitrogen reduction (Li-NRR) represents a promising approach for continuous-flow ammonia electrosynthesis, coupling nitrogen reduction with hydrogen oxidation⁴. However, tetrahydrofuran (THF), commonly used as a solvent, impedes long-term ammonia production due to polymerization and volatility issues. Here we show that a chain ether-based electrolyte enables long-term continuous ammonia synthesis. We find that a chain ether-based solvent exhibits non-polymerization properties, a high boiling point (162 °C), and forms a compact solid-electrolyte interphase (SEI) layer on the gas diffusion electrode (GDE), facilitating ammonia release in the gas phase and ensuring electrolyte stability. We demonstrate 300 hours continuous operation in a flow electrolyzer with 25 cm² electrode at 1 bar and room temperature, and achieve a current-to-ammonia efficiency of 64 ± 1% with unprecedented gas phase ammonia content of ~98%. Our work highlights the crucial role of the solvent in long-term continuous ammonia synthesis.

30 The Li-NRR in non-aqueous electrolytes was first reported in 1930 by Fichter *et al.*⁵ using an
31 alcohol solvent with lithium chloride at 1000 bar N₂ and was investigated by Tsuneto *et al.*^{6,7} in
32 1993 using a ring ether-based solvent (i.e., THF) with lithium perchlorate. Since our group first
33 validated that nitrogen molecules are indeed activated in the Li-NRR process to produce ammonia
34 through a rigorous procedure⁸, different strategies have been reported to improve the ammonia
35 faradaic efficiency (FE)⁹⁻¹¹, current density^{12,13}, and stability¹⁴. Nevertheless, most Li-NRR
36 investigations have been conducted using batch reactors, which present challenges due to the use
37 of sacrificial solvents as proton donors and difficulties in scaling up production.

38 A promising strategy to establish a sustainable hydrogen source for ammonia synthesis involves
39 incorporating a hydrogen oxidation reaction (HOR) on the anode^{4,11,15}. Lazouski et al. first
40 proposed using a stainless-steel cloth (SSC) as the GDE for Li-NRR and using Pt-coated SSC for
41 HOR in a three-compartment cell¹⁵. Our recent work highlights the use of a PtAu alloy catalyst for
42 HOR in organic electrolytes⁴, and demonstrates a 10-hour continuous operation that achieved
43 ammonia FE of 61%. Nonetheless, all previous reports have been unable to achieve long-term
44 continuous-flow ammonia electrosynthesis beyond 10 hours and to demonstrate ammonia
45 production at a gram scale (Fig. 1a). One of the main reasons is the polymerization and volatility
46 of THF^{6, 8-19} (Fig. 1b). Further, severe solvent oxidation phenomena were observed due to the use
47 of a sacrificial agent¹⁶. In a continuous-flow reactor, the Li⁺ is reduced on the cathode to form
48 metallic Li and then reacts with N₂, followed by protonation and subsequent production of
49 ammonia (Fig. 1c). The proton is generated from HOR on the anode and delivered by a proton
50 shuttle, e.g., ethanol (EtOH). However, the ring-opening polymerization²⁰ and low boiling point
51 of 66 °C of THF impedes the long-term continuous-flow operation. Therefore, new solvents are
52 highly desirable for the long-term continuous ammonia synthesis (Fig. 1c): (I) The solvent should
53 enable noticeable solubility of the lithium salt, ensuring high ionic conductivity and facilitating
54 lithium plating. (II) The solvent must be compatible with metallic lithium to form a suitable SEI
55 layer, while also being compatible with a proton shuttle to facilitate the delivery of protons
56 generated from the HOR. (III) The presence of ammonia in the gas phase is highly desirable, which
57 allows for easier and more cost-effective separation. To achieve this, the solvent-induced SEI on
58 the GDE needs to be compact without obstructing the release of ammonia into the gas phase. (IV)
59 To enhance long-term stability, the solvent must possess both non-polymerization capabilities to
60 prevent electrolyte degradation and a high boiling point to avoid electrolyte evaporation.

61 Solvent effects for Li-NRR

62 To assess the capability of different ether-based solvents for Li-NRR, especially two kinds of ring
63 ether-based solvents (THF and 1, 3-dioxolane, named DOL) and two kinds of chain ether-based
64 solvents (dimethoxyethane, named DME, and diethylene glycol dimethyl ether, named DG), all
65 experiments were performed using a continuous-flow reactor with a 25 cm² effective area GDE,
66 as described in Methods section and Supplementary Fig. 1. It should be pointed out that although
67 DG has been reported for Li-NRR with different lithium salt (i.e., lithium triflate) by our group²¹,
68 the micro-chip-based cell for electrochemistry mass spectrometry set-up is far away from the
69 continuous-flow reactor. Our previous study has showcased a potential cycling strategy^{4,14} (1 min
70 for Li deposition following by 1 min resting at open circuit voltage, defined as cycling in this work)
71 that can improve the performance of Li-NRR using THF. However, we found that controlling the
72 resting potential (defined as controlled cycling) rather than the resting time is critical for the
73 improved performance using DME and DG, because the ending potential above the Li deposition
74 potential directly indicates the consumption of metallic lithium or lithium nitride species
75 (Supplementary Fig. 2-9).

76 Li-NRR coupled with HOR in the continuous-flow reactor with controlled cycling leads to the
77 average anode potential staying around 0.6 V versus Pt, and a total cell voltage of 4.0 V for DG
78 (Fig. 2a). Compared with THF, DME and DG exhibit the lower electrolyte resistance
79 (Supplementary Fig. 10). The promotional effect of controlled cycling is observed for both DME
80 and DG (Fig. 2b, Supplementary Fig. 2-7). At the optimal EtOH concentration with controlled
81 cycling, a FE of $81 \pm 1\%$ and $76 \pm 1\%$ was achieved using DME and DG, respectively, which are
82 higher than that of THF ($63 \pm 1\%$ FE). In the case of THF with cycling, a relatively low amount
83 of metallic Li might be plated when applying potential, allowing it to be fully utilized for
84 nitridation and protonation within 1 minute of open circuit voltage (OCV). This essentially
85 achieves a comparable efficiency to controlled cycling. Moreover, more than 60% of produced
86 ammonia is distributed in the gas phase using DG with controlled cycling (Fig. 2c, Supplementary
87 Table 1). Compared with controlled cycling, the non-controlled cycling could potentially lead to a
88 relatively thicker SEI layer and further induce the ammonia trapped in the electrolyte. The
89 compatibility of DME and DG with EtOH were also proved by D₂ isotope studies in the
90 continuous-flow reactor (Supplementary Fig. 11, 12). An operando mass spectrometry experiment
91 of 28 hours was further carried out using DG for monitoring the on-site hydrogen and ammonia
92 production in the gas phase (Fig. 2d). After first switching from OCV to the lithium deposition
93 potential, ammonia starts to be formed and produced continuously over the duration.

94

95 **Stability of electrolyte**

96 Regarding the capability of DOL for Li-NRR, the initially liquid LiBF₄-DOL electrolyte
97 transitions into a gel-state electrolyte after 2 hours, even without electrochemistry (Fig. 3a). New
98 hydrogen peaks in accordance with the structure of polyDOL are also observed in the nuclear
99 magnetic resonance (NMR) analysis^{22,23}. The LiBF₄-THF electrolyte is also transformed to a gel-
100 state electrolyte (Fig. 3b) after a 14-hour Li-NRR operation in the continuous-flow reactor due to
101 the THF polymerization^{24,25}. It has been reported that the breaking of the C-O bond is the cause of
102 the THF polymerization²⁶. Based on extended *ab initio* molecular dynamics (AIMD) simulations
103 of THF with and without dissolved lithium salt, we have provided additional evidence for this
104 picture. We show that the C-O radial distribution function exhibits a stretched C-O bond in the
105 presence of lithium salt (Supplementary Fig. 13, 14), indicating a weakened C-O bond and hence
106 more facile C-O bond breaking.

107 For the LiBF₄-DG electrolyte, on the other hand, no visible change can be observed over 300-hour
108 continuous Li-NRR operation (Fig. 3c). The electrochemical oxidation of THF, DME, and DG in
109 an aqueous electrolyte also indicates the superior stability of DG and DME (Supplementary Fig.
110 15)²⁷⁻²⁹. These findings emphasize the stability of DG as an efficient solvent in practical Li-NRR
111 process. More detailed investigations of the long-term continuous Li-NRR operation are discussed
112 in the following section.

113 X-ray photoelectron spectrometer (XPS), X-ray diffraction (XRD) and scanning electron
114 microscopy (SEM) were used to investigate the key role of the solvent in the SEI formation
115 (Supplementary Fig. 16-18). The deposited layer using DG shows particle-like deposits, appearing
116 thin and uniform, while the deposited layer using THF not only covered the GDE but also was
117 interconnected and blocked its pores (Fig. 3d, e, Supplementary Fig. 19-21). Cryogenic
118 transmission electron microscopy (cryo-TEM) images further confirmed the presence of
119 nanoparticles with a mean size of 13 ± 2 nm in the deposited layer using DG (Supplementary Fig.
120 20). After 100 and 300 hours of operation, increased particle-like deposits covered the electrodes,
121 with nanoparticles sizes growing to 16 ± 3 and 22 ± 3 nm, respectively. The deposited layer reached
122 a thickness of ~ 240 nm after 300 hours (Supplementary Fig. 21), forming a compact SEI mainly
123 composed of nanoparticles ranging from 13-22 nm over 300 hours. Contrary to these results, the
124 deposit on the GDE using THF comprised of particles averaging 433 ± 78 nm in size after only

125 2.4 hours (Supplementary Fig. 22). High resolution cryo-TEM (HR-TEM) images revealed a
126 complex structure of the SEI layer using DG (Supplementary Fig. 23), featuring nanoscale regions
127 of crystalline species. Selected area electron diffraction (SAED), HR-TEM, and SEM with energy
128 dispersive x-ray spectroscopy also implied that these regions consist of LiF (Supplementary Fig.
129 23, 24). Further, the main inorganic component of LiF in the different deposit layers is confirmed
130 by XRD and depth-profiling XPS (Supplementary Fig. 25-30).

131 Considering the trace amount of water that is typically present in the fresh electrolyte, the effect
132 of H₂O concentration is also investigated (Fig. 4, Supplementary Fig. 31-33). The electrochemical
133 performance and FE do not exhibit obvious changes as the H₂O concentration increased from 1.6
134 to 16.1 mM with optimal EtOH concentration (25.8 mM) in DG (Fig. 4a, Supplementary Fig. 31),
135 which indicates a certain amount of H₂O tolerance (1.6 to 16.2 mM) in the system. However, the
136 FE and stability notably decline with H₂O concentrations surpassing 20.9 mM (Fig. 4a,
137 Supplementary Fig. 32). Specifically, the resting time for the cathode potential to return to -2.5 V
138 intensively increased, accompanied by a dramatic FE drop to $7 \pm 1\%$. This is potentially caused
139 by a passivated SEI layer due to excessive H₂O content, which blocked the consumption of metallic
140 lithium. The phenomenon regarding increased resting time is more notable as the H₂O
141 concentration further increased to ~31.6 mM. Moreover, without the presence of EtOH, less
142 ammonia produced and most of the ammonia is present in the electrolyte rather than in the gas
143 phase (Fig. 4b). It indicates that water alone, without EtOH, cannot sustain the long-term
144 continuous ammonia electrosynthesis.

146 **Long-term operation**

147 The long-term stability in a continuous-flow reactor was evaluated with controlled cycling
148 (Supplementary Fig. 34-39, Table 2-7). The anode potential started to increase after 10 hours with
149 THF, and kept increasing to 1.68 V after 14.4 hours until we manually terminated the reaction due
150 to severe THF evaporation and polymerization (Fig. 5a). DME provides better stability but also
151 exhibits a similar anode potential increase after 26 hours, and electrolyte loss due to DME
152 evaporation (boiling point of 85 °C). On the contrary, four independent 300-hour continuous
153 operations were enabled by using DG (Fig. 5b), and the average anode potential is less than 1 V
154 over the whole duration. The accelerated passed charge over time is ascribed to the reduced time
155 at resting periods, likely linked to SEI buildup and stabilization. Electrolyte water content, pH, and

156 temperature may also affect SEI buildup and stabilization. An ammonia FE of 64% was achieved
157 using DG after 300-hour operation with a slight degradation towards the end (Fig. 5c), while THF
158 obtained 28% FE after 14 hours and DME obtained 48% FE after 27 hours. The severe ammonia
159 FE decay using THF is due to electrolyte degradation from THF evaporation, polymerization, and
160 high anode potential leading to THF oxidation. After 300-hour operation, 3 mL DG had evaporated
161 from 120 mL electrolyte, while 90 mL THF had evaporated only after 14 hours. In addition, 5%
162 EtOH was consumed, and no obvious Li and B consumption was observed over 300-hour operation
163 (Supplementary Fig. 40-42). Pre-saturating the N₂ and H₂ with solvent could mitigate solvent loss
164 in long-term experiments, and is worth considering for scale-up.

165 The ammonia distribution in the gas phase and electrolyte is found to be strongly dependent on the
166 type of solvent used (Fig. 5d, Supplementary Fig. 43). Specifically, ~98% of ammonia
167 accumulated in the gas phase for DG after 300 hours. The ammonia concentration in the electrolyte
168 did not reach a point of saturation but more ammonia began distributing in the gas phase
169 (Supplementary Fig. 44), possibly due to an ammonia concentration gradient in the electrolyte.
170 We obtained more than 4.6 g of ammonia in total after 300 hours, and 4.5 g of ammonia in the gas
171 phase. This marks the first Li-NRR demonstration for ammonia production at a gram scale, with
172 over 95% of the produced ammonia observed in the gas phase, a novel achievement. Stability, FEs,
173 and energy efficiencies (EEs) of previous publications are summarized in Fig. 5e and
174 Supplementary Table 8 for comparison. We achieved 17% EE and 300 hours stability using DG,
175 both are highest among all the reported results. Notably, theoretical maximal EE for Li-NRR
176 process is ~28% based on our previous calculation⁴. Notably, reported EEs in continuous-flow
177 reactors include H₂ as the proton source, whereas pseudo-EEs in batch reactors exclude the energy
178 for H₂ synthesis, without demonstration of proton origin from hydrogen or sacrificial agents.

179 The findings presented here mark progress in identifying stable solvents for achieving long-term
180 stability and optimal product distribution in continuous-flow ammonia electrosynthesis via Li-
181 NRR. We also demonstrate the feasibility of using high surface area GDE in the continuous-flow
182 reactor to increase the current density from -6 to -60 mA cm⁻² (Supplementary Fig. 45). While
183 significant, this doesn't address all Li-NRR challenges for industrial application. Achieving
184 industrial relevant current densities demands optimizing GDE, electrolyte formulation, cycling
185 procedure, and reactor design. Future Li-NRR research should target high FE and EE at industrial

186 relevant current densities while maintaining long-term stability and gas-phase ammonia in pilot-
187 scale flow cells.

188

189 References

- 190 1. Christensen, C.H., Johannessen, T., Sørensen, R.Z. & Nørskov, J.K. Towards an ammonia-
191 mediated hydrogen economy? *Catal. Today* **111**, 140-144 (2006).
- 192 2. MacFarlane, D.R. et al. A roadmap to the ammonia economy. *Joule* **4**, 1186-1205 (2020).
- 193 3. Iriawan, H. et al. Methods for nitrogen activation by reduction and oxidation. *Nat. Rev.*
194 *Methods Primers* **1**, 56 (2021).
- 195 4. Fu, X. et al. Continuous-flow electrosynthesis of ammonia by nitrogen reduction and
196 hydrogen oxidation. *Science* **379**, 707-712 (2023).
- 197 5. Fichter, F., Girard, P. & Erlenmeyer, H. Elektrolytische Bindung von komprimiertem
198 Stickstoff bei gewöhnlicher Temperatur. *Helv. Chim. Acta* **13**, 1228-1236 (1930).
- 199 6. Tsuneto, A., Kudo, A. & Sakata, T. Efficient electrochemical reduction of N₂ to NH₃
200 catalyzed by lithium. *Chem. Lett.* **22**, 851-854 (1993).
- 201 7. Tsuneto, A., Kudo, A. & Sakata, T. Lithium-mediated electrochemical reduction of high
202 pressure N₂ to NH₃. *J. Electroanal. Chem.* **367**, 183-188 (1994).
- 203 8. Andersen, S.Z. et al. A rigorous electrochemical ammonia synthesis protocol with
204 quantitative isotope measurements. *Nature* **570**, 504-508 (2019).
- 205 9. Du, H.-L. et al. Electroreduction of nitrogen with almost 100% current-to-ammonia
206 efficiency. *Nature* **609**, 722-727 (2022).
- 207 10. Li, K. et al. Enhancement of lithium-mediated ammonia synthesis by addition of oxygen.
208 *Science* **374**, 1593-1597 (2021).
- 209 11. Suryanto Bryan, H.R. et al. Nitrogen reduction to ammonia at high efficiency and rates
210 based on a phosphonium proton shuttle. *Science* **372**, 1187-1191 (2021).
- 211 12. Li, K. et al. Increasing current density of Li-mediated ammonia synthesis with high surface
212 area copper electrodes. *ACS Energy Lett.* **7**, 36-41 (2022).
- 213 13. Li, S. et al. Electrosynthesis of ammonia with high selectivity and high rates via
214 engineering of the solid-electrolyte interphase. *Joule* **6**, 2083-2101 (2022).
- 215 14. Andersen, S.Z. et al. Increasing stability, efficiency, and fundamental understanding of
216 lithium-mediated electrochemical nitrogen reduction. *Energy Environ. Sci.* **13**, 4291-4300
217 (2020).
- 218 15. Lazouski, N., Chung, M., Williams, K., Gala, M.L. & Manthiram, K. Non-aqueous gas
219 diffusion electrodes for rapid ammonia synthesis from nitrogen and water-splitting-derived
220 hydrogen. *Nat. Catal.* **3**, 463-469 (2020).
- 221 16. Du, H.-L. et al. The chemistry of proton carriers in high-performance lithium-mediated
222 ammonia electrosynthesis. *Energy Environ. Sci.* **16**, 1082-1090 (2023).
- 223 17. Lazouski, N., Schiffer, Z.J., Williams, K. & Manthiram, K. Understanding continuous
224 lithium-mediated electrochemical nitrogen reduction. *Joule* **3**, 1127-1139 (2019).
- 225 18. Cai, X. et al. Lithium-mediated electrochemical nitrogen reduction: mechanistic insights
226 to enhance performance. *iScience* **24**, 103105 (2021).
- 227 19. Steinberg, K. et al. Imaging of nitrogen fixation at lithium solid electrolyte interphases via
228 cryo-electron microscopy. *Nat. Energy* **8**, 138-148 (2023).
- 229 20. Sažinas, R. et al. Oxygen-enhanced chemical stability of lithium-mediated electrochemical
230 ammonia synthesis. *J. Phys. Chem. Lett.* **13**, 4605-4611 (2022).

- 231 21. Kreml, K. et al. Quantitative operando detection of electro synthesized ammonia using
232 mass spectrometry. *ChemElectroChem* **9**, e202101713 (2022).
- 233 22. Zhao, Q., Liu, X., Stalin, S., Khan, K. & Archer, L.A. Solid-state polymer electrolytes with
234 in-built fast interfacial transport for secondary lithium batteries. *Nat. Energy* **4**, 365-373
235 (2019).
- 236 23. Liu, F.-Q. et al. Upgrading traditional liquid electrolyte via in situ gelation for future
237 lithium metal batteries. *Sci. Adv.* **4**, eaat5383 (2018).
- 238 24. Seto, R., Yamada, S., Matsumoto, K. & Endo, T. Synthesis of block copolymers through
239 unpolung or treatment of propagating end of living cationic polytetrahydrofuran. *Polym.*
240 *Bull.* **76**, 3355-3370 (2019).
- 241 25. Aouissi, A., Al-Deyab, S.S. & Al-Shahri, H. The cationic ring-opening polymerization of
242 tetrahydrofuran with 12-tungstophosphoric acid. *Molecules* **15**, 1398-1407 (2010).
- 243 26. Cataldo, F. Iodine: a ring opening polymerization catalyst for tetrahydrofuran. *Eur. Polym.*
244 *J.* **32**, 1297-1302 (1996).
- 245 27. Avgousti, C., Georgolios, N., Kyriacou, G. & Ritzoulis, G. The electrochemical oxidation
246 of tetrahydrofuran in sulphuric acid solution. *Electrochim. Acta* **44**, 3295-3301 (1999).
- 247 28. Zhang, L.Y., Gong, Y., Liu, H., Yuan, W. & Liu, Z. Ultrasmall and uniform Pt₃Au clusters
248 strongly suppress Ostwald ripening for efficient ethanol oxidation. *Electrochem. Commun.*
249 **84**, 1-5 (2017).
- 250 29. Horwitz, G., Calvo, E.J., Méndez De Leo, L.P. & de la Llave, E. Electrochemical
251 stability of glyme-based electrolytes for Li-O₂ batteries studied by in situ infrared
252 spectroscopy. *Phys. Chem. Chem. Phys.* **22**, 16615-16623 (2020).

253

254 **Figure legends**

255 **Fig. 1 Schematic illustration for long-term electrochemical ammonia synthesis.** **a**, Produced
256 ammonia versus stability reported in batch reactors (blue and purple squares)^{8-13,17,18}, continuous-
257 flow reactors (orange circle)^{4,15}, and this work (red circle). **b**, Overview of solvent developed for
258 lithium-mediated ammonia synthesis. **c**, Comparison of long-term continuous ammonia synthesis
259 with different solvents. The solvent greatly affects the electrolyte stability and the derived deposit
260 including the SEI on the gas diffusion electrode, as well as the ammonia distribution in the gas
261 phase.

262

263 **Fig.2 Investigation of different solvents in a continuous-flow reactor.** **a**, Chronopotentiometry
264 at the current density of -6 mA cm⁻² with DG and EtOH concentration of 43.0 mM. All reported
265 potentials are presented without ohmic drop correction. **b**, The effect of EtOH concentration,
266 controlled cycling, and solvent on the ammonia FE. **c**, The effect of controlled cycling and solvent
267 on the ammonia distribution in the electrolyte, gas phase, and electrode deposits at the EtOH
268 concentration of 43.0 mM. **d**, Operando mass spectrometry of the cathodic gas products over 28
269 hours. The upper panel is the applied potentials during the controlled cycling at the current density
270 of -6 mA cm⁻². The bottom panel is the measured ammonia and hydrogen products. Error bars
271 show the standard deviation from at least three independent experiments.

272

273 **Fig. 3 Structure analysis of the solvent and gas diffusion electrode for the continuous**
274 **ammonia electrosynthesis.** **a**, Hydrogen NMR spectra of the DOL-based electrolyte before and
275 after 2 hours of rest. **b**, **c**, Hydrogen NMR spectra of the THF-based electrolyte after 14 hours (**b**)
276 and diglyme-based electrolyte after 300 hours (**c**). Insets in (**a**) and (**b**) are the corresponding digital

277 photographs of the liquid electrolyte before and after the reaction. Insets in (c) are the
278 corresponding digital photographs of the liquid electrolyte during the reaction. **d, e**, Representative
279 SEM images of the gas diffusion electrode after using THF-based (**d**) and DG-based (**e**) electrolyte
280 for continuous ammonia electrosynthesis with the same passed charge of 700 C.

281
282 **Fig. 4 The effect of water concentration.** **a, b**, The effect of water concentration on the ammonia
283 FE (**a**) and ammonia distribution in the electrolyte, gas phase, and electrode deposits (**b**). With or
284 no EtOH shown in (**a**) and (**b**) means electrolyte with optimal EtOH concentration of 25.8 mM or
285 without EtOH. Error bars show the standard deviation from at least three independent experiments.

286
287 **Fig. 5 Long-term ammonia electrosynthesis in continuous-flow reactor.** **a, b**, Long-term
288 ammonia synthesis with controlled potential cycling at -6 mA cm^{-2} using THF, DME (**a**), and DG.
289 (**b**). **c, d**, The evolution of the ammonia FE (**c**) and ammonia distribution in gas phase and
290 electrolyte (**d**) over passed charge for the long-term experiments using different solvents. **e**,
291 Comparison of the stability, FE and EE with literature results using batch reactor with THF (purple
292 boxes)^{8-15,17,18}, continuous-flow reactor with THF (brown cylinder)^{4,15} and DG (red cylinder, this
293 work).

294 **Methods**

295 **Preparation of electrodes**

296
297 The 36 cm^2 316 stainless-steel cloth (SSC, McMaster-Carr, 500×500 mesh, pore size: $30 \mu\text{m}$)
298 was used as the working electrode (WE). The PtAu catalyst electrodeposited on the same type of
299 SSC electrode (PtAu/SSC) was prepared by the hydrogen bubble method. Prior to use, the SSC
300 was washed with acetone and ethanol three times. To achieve uniform PtAu electrodeposition, the
301 two Pt meshes (Goodfellow, $1.5 \text{ cm} \times 1.5 \text{ cm}$, 99.9 %) were electrically connected and used as a
302 split counter electrode, where the working electrode (SSC) was placed in the middle between
303 counter electrodes. The 10 mM $\text{H}_2\text{PtCl}_6 \cdot 6\text{H}_2\text{O}$ (Sigma Aldrich, ACS reagent) with 10 mM
304 $\text{HAuCl}_4 \cdot 3\text{H}_2\text{O}$ (Sigma Aldrich, 99%) in 3 M H_2SO_4 (Sigma Aldrich, 99.999%) solution was used
305 as an electrolyte for electrodeposition PtAu/SSC. A current density of -0.2 A cm^{-2} was applied for
306 2 min, leading to high surface area structures of PtAu on the SSC. The 0.4 M CuSO_4 (Merck, 98%)
307 in 1.5 M H_2SO_4 (Sigma Aldrich, 99.999%) solution was used as an electrolyte for electrodeposition
308 Cu/SSC. A current density of -1.0 A cm^{-2} was applied for 1 min, leading to high surface area
309 structures of Cu on the SSC. After the electrodeposition, the electrodes were rinsed in EtOH and
310 ultra-pure water ($18.2 \text{ M}\Omega$ resistivity, Millipore, Synergy UV system) several times to remove all
311 residual electrolytes.

312 **Electrochemical experiments in a continuous-flow reactor**

313 Electrochemical ammonia synthesis was conducted in a three-chamber flow cell (Supplementary
314 Fig. 1). The dimension of the flow cell was $10.7 \text{ cm} \times 10.7 \text{ cm} \times 5.1 \text{ cm}$. The effective area of the
315 flow field was 25 cm^2 . The size of gas flow channels was 1 mm. The thickness of the central
316 electrolyte chamber is 4 mm. The SSC (500×500 mesh, pore size: $30 \mu\text{m}$) was used as WE. As-
317 prepared PtAu/SSC was used as the counter electrode (CE). The pseudo reference electrode (RE)
318 was a Pt wire (Goodfellow, 99.99 %, diameter: 0.5 mm). Before electrochemical tests, the Pt wire
319 was flame annealed. The N_2 (5.0, Air Liquide) and H_2 (5.0, Air Liquide) gas flow rates were
320 controlled using a mass flow controller (Brooks Instrument) and set to 5-75 sccm. The N_2 and H_2
321 used in the experiments were cleaned by purifiers (NuPure) and all labile N-containing compounds

322 can be down to parts per trillion by volume (ppt-v) level. The LiBF₄ (Sigma Aldrich, ≥ 98%,
323 anhydrous) was dried at 120 °C for 48 h in a vacuum oven before use. EtOH (Honeywell,
324 anhydrous) was dried with 3 Å molecular sieves. Electrolyte solution consisted of 1 M LiBF₄ in
325 solvent (THF, anhydrous, >99.9%, inhibitor-free, Sigma Aldrich, DME or DG, anhydrous, 99.5%,
326 Sigma Aldrich) and 0-172.0 mM EtOH was prepared in an Ar glovebox (Vigor). A peristaltic pump
327 (Baoding Zhunze Precision Pump Manufacturing Co., ltd.) was used to control the flow rate of the
328 electrolytes at 1.0 ml min⁻¹ (Supplementary Fig. 46). The electrolyte without any gas pre-saturation
329 was pumped in a loop through the cell and a container. 120 mL electrolyte was used for all the
330 long-term experiments considering the fast evaporation of THF. 60 or 30 mL electrolyte was used
331 for all the short-term experiments. Around 10 sccm N₂ gas is flowed into the container to avoid air
332 exposure of the electrolyte. 75 sccm of N₂ and H₂ gas flow rates were used for all the short-term
333 experiments, and 5 sccm of N₂ and H₂ gas flow rates can be used for the long-term experiments.
334 The pressure gradient (*i.e.* 15 mbar) between the gas inlet and outlet of the flow cell was modulated
335 by a 10.5 centimeters water column (50 mL) above the gas. 10 mM of H₂SO₄ (Sigma Aldrich,
336 99.999%) or HCl (Sigma Aldrich, Suprapur) solution was used as an NH₃ trap solution. Generally,
337 1.0-2.6 mM of water content was measured in the as-prepared electrolyte via Karl Fischer Titration
338 (831 KF Coulometer and 728 Stirrer, Metrohm).

339 Prior to injection of electrolyte into the liquid chamber, the purified N₂ and H₂ (75 sccm) were
340 introduced into the empty assembled flow cell for at least 30 min. Afterward, the electrolyte
341 solution was injected into the cell in N₂ and H₂ atmospheres. The electrochemistry experiments
342 were performed using a BioLogic Potentiostat (VMP2). The resistance between the WE and RE
343 was measured using the potentiostatic electrochemical impedance spectroscopy. The linear sweep
344 voltammetry was recorded from the OCV until lithium reduction is clearly seen. Subsequently,
345 Chronopotentiometry (CP) was measured. In the normal cycling, -6 mA cm⁻² was applied for 1
346 min and then 0 mA cm⁻² for 1 min. In the controlled cycling, -6 mA cm⁻² was applied for 1 min
347 and then 0 mA cm⁻² is kept until the cathode potential reached the target potential, *e.g.*, -2.8 to -2.2
348 V, typically -2.5 V. 297 C of charge was passed for each short-term experiment unless otherwise
349 specified. All experiments were conducted at room temperature and 1 bar. Typically, flow cell
350 experiments were performed in a fume hood. For analysis of the SEI on the working electrode, the
351 flow cell was run in an Ar glovebox. When the experiment was finished, produced NH₃ was
352 distributed in three parts, (1) gas-phase NH₃ trapped in 10 mM of H₂SO₄ or HCl, (2) NH₃ trapped
353 in the electrolyte, and (3) NH₃ trapped in the electrode deposits. Typically, 120 ml of ultra-pure
354 water was used to dissolve the electrode deposits to release trapped NH₃, since H₂O can react with
355 intermediate nitrogen species (*e.g.* Li₃N) in the electrode deposits to produce NH₃. After the short-
356 term experiment, the water content of the electrolyte was increased to 5.2-7.8 mM. The water
357 content of the electrolyte was increased to 13.6 to 14.0 mM after 300 hours experiment.

358 For the experiment operated at -60 mA cm⁻² using 25 cm² high surface area Cu/SSC, the thickness
359 of the central electrolyte chamber is 1 mm, and the electrolyte solution consisted of 1 M LiBF₄ in
360 DG and 172.0 mM EtOH. In the controlled cycling, -60 mA cm⁻² was applied for 1 s and then 0
361 mA cm⁻² is kept until the cathode potential reached -2.5 V. All the other conditions are the same as
362 the experiments operated at -6 mA cm⁻². The electrode used for higher current densities is made of
363 highly structured Cu (with particles diameter of 1 to 3 μm) self-assembled on the SSC
364 (Supplementary Fig. 45a, b). Based on our developed kinetic model that describes the mechanism
365 of Li-NRR¹⁴, the H⁺, N₂, and Li⁺ diffusion rates also need to be rebalanced at high current density
366 to maintain the high ammonia FE. Therefore, the EtOH concentration is increased from 43.0 (at -
367 6 mA cm⁻²) to 172.0 mM at -60 mA cm⁻², and the deposition time in the controlled cycling
368 procedure is decreased from 1 min to 1 s to avoid thick lithium deposits. The anode potential and
369 cell voltage stays stable around 0.7 V (versus Pt) and 4.3 V at -60 mA cm⁻², respectively

(Supplementary Fig. 45c-e). Notably, achieving 297 C takes only 29 minutes at -60 mA cm^{-2} , contrasting with 260 minutes at -6 mA cm^{-2} , indicating a comparable ratio of resting and deposition periods at these two current densities. Comparable FE and gas-phase ammonia were achieved at -60 mA cm^{-2} compared with -6 mA cm^{-2} (Supplementary Fig. 45f). The electrolyte formulation, high surface area GDE, and continuous-flow reactor reported in the present work are not the final version for practical or commercial use. However, these results serve as a promising foundation for further enhancements in current density through systematic optimization of the above parameters.

D₂ oxidation experiment via operando mass spectrometry

Mass spectrometry (MS) measurements were collected with a QMG 422, using a 100 mm long QMA 120 quadrupole mass filter (QMS) from Balzers. The QMS was optimized for soft ionization measurements at 26 eV ionization energy, ensuring minimum cracking patterns in the mass spectra, while allowing for a decent signal. The MS is placed downstream on the N₂ flow from the cathode side of the flow cell (Supplementary Fig. 47). This allows for *operando* measurements of the flow cell operation and performance. The connecting gas line is heat traced to 100 °C, to avoid sticking ammonia to the inner tube walls and increase collection efficiency and time resolution. The continuous gas collection is through a 1 μm flow calibrated orifice from Lenox Laser. Measurements with electrolytes in the flow cell are collected under a low vacuum of typically 2.4×10^{-6} mbar, while the vacuum chamber is heated to 120 °C. The vacuum is sustained by a HiPace 300 H Turbo Pump from Pfeiffer Vacuum. The electrochemical reaction was performed as the same condition as the aforementioned continuous-flow reactor. Deuterium (D₂, 99.8 atom% D, 4.5N purity) and nitrogen (N₂, 5N purity) flow rates were controlled with mass flow controllers (Brooks Instrument), and both were set to 50 sccm. D₂ outlet gas was passed directly through a water column, whereas the N₂ gas outlet was flowed by the mass spectrometer before passing through a water column. Once both gases and electrolytes were flowing, the mass spectrometer was started and measured on the N₂ gas outlet. The baseline mass signals were measured starting from the OCV. More details on the calibration curve for mass spectrometry quantification can be found in our previous work⁴.

THF, DME, and DG oxidation experiments in aqueous electrolyte

To evaluate the electrochemical stability of THF, DME, and DG on the PtAu anode catalysts, oxidation experiments in an aqueous electrolyte were carried out in a custom-made three-electrode glass cell using the rotating disk electrode method. The Hg/Hg₂SO₄ reference electrode was calibrated before the electrochemistry test and a Pt wire was used as a counter electrode. The working electrode (PtAu/Ti) was obtained from electrodeposited PtAu on a titanium stub ($\phi = 5 \text{ mm}$, 0.196 cm^2). To prepare the PtAu/Ti electrode, an electrolyte of 10 mM H₂PtCl₆·6H₂O (Sigma Aldrich, ACS reagent) with 10 mM HAuCl₄·3H₂O (Sigma Aldrich, 99%) in 3 M H₂SO₄ (Sigma Aldrich, 99.999%) was used. A current density of -1.0 A cm^{-2} was applied for 2 min in which rigorous hydrogen evolution and metal deposition took place at the same time with 2500 revolutions per minute. The cyclic voltammetry curve was recorded between 0 and 1.4 V vs RHE at 50 mV s^{-1} in Ar-saturated 0.1 M H₂SO₄. THF, DME, and DG oxidation activity were evaluated in Ar-saturated 0.1 M H₂SO₄ with 0.1 M THF or 0.1 M DME or 0.1 M DG electrolyte with a scan rate of 50 mV s^{-1} .

Quantification of ammonia

Produced ammonia was quantified by ion chromatography (IC, Metrohm). The materials of connection tubes, pressure screws, capillaries, and injection needles are PEEK or PTFE (THF-resistant materials). The cation column (Metrosep C6) made by silica gel with carboxyl groups

416 was used as a high-capacity separation column. The eluent (mobile phase) was 3.3 mM HNO₃
417 (Sigma Aldrich, Suprapur) solution with 1.35 M acetone (i.e., 10 vol%, Sigma Aldrich, ≥ 99.9%).
418 The eluent flow rate was 0.9 ml min⁻¹. Before use, the eluent was degassed for 30 min to prevent
419 gas bubbles in the high-pressure pump. The sample injection volume was 20 μL. The data
420 acquisition time was 20 min. Ammonium chloride (Sigma Aldrich, 99.998%) solution was used to
421 make the NH₃ calibration curve shown in our previous work⁴. The solution with ammonia was
422 diluted accordingly with ultra-pure water within the range of calibration curve. The sample or
423 diluted sample contains any visible particles was pre-treated by a filter syringe with a PTFE filter
424 membrane (Whatman Puradisc, 0.45 μm) to remove the insoluble substance before testing IC. The
425 ion concentration is proportional to the peak area. All the FE were calculated by the following
426 equation:

$$427 \quad \text{FE} = 3 \times F \times (c_1 \times V_1 + c_2 \times V_2 + c_3 \times V_3) / Q \quad (1)$$

428 where 3 is the number of electrons transferred for each mole of NH₃, F is the Faraday constant, *c*₁,
429 *c*₂, *c*₃ is the concentration of produced ammonia in the electrolyte, gas-phase trapped solution, and
430 electrode deposits dissolved solution, respectively, *V*₁, *V*₂, *V*₃ is the corresponding solution volume,
431 respectively, and *Q* is the total passed charge. Details on the calculation method for the EEs,
432 including the pseudo-EEs can be found in our previous work⁴.

433 **Characterization**

434 XPS (ThermoScientific Thetaprobe), SEM (Quanta FEG 250) and XRD (Malvern Panalytical
435 Empyrean X-ray diffractometer) were used to investigate the SEI on the electrode after
436 electrochemistry. The flow cell experiments were performed in an Ar-filled glovebox
437 (Supplementary Fig. 48) and corresponding transfer system was used to minimize the air exposure
438 of the electrodes (Supplementary Fig. 16-18). All the electrodes were dried after wash treatment
439 (gently dip into the corresponding solvent for 5 times) in the glovebox before characterization,
440 unless otherwise specified. XPS was conducted with an Al Kα x-ray source and base pressure
441 below 9.0 × 10⁻¹⁰ mbar. The ion gun in etching mode and flood gun in charge neutralization mode
442 were used during the measurement with a chamber pressure of 2.0 × 10⁻⁷ mbar by flowing Ar gas
443 (99.9999%, Air Liquide). The ion gun was run using 4 kV and 1 μA mode with scanning size of
444 2 × 2 mm². The spot size of 400 μm were used. All the survey spectra were recorded with step size
445 of 1.0 eV and dwell time of 50 ms at pass energy of 200 eV (Supplementary Fig. 30). High
446 resolution elemental spectra were recorded with step size of 0.1 eV and dwell time of 50 ms at
447 pass energy of 200 eV. All the spectra were acquired and analyzed by Thermo Avantage (v5.9925)
448 by Thermo Fisher Scientific. All the background were determined using Shirley mode and fitted
449 using Powell algorithm. The F 1s spectra of all the electrodes show the two peaks that attributed
450 to LiF and Li_xBF_y^{13,19}, respectively (Supplementary Fig. 26-29). The ratio of the LiF signal
451 increases as the etching time increases, which indicates a LiF-enriched SEI layer on the GDE. The
452 prominent O 1s C-O peak and C 1s C-C and C-O signals reveal the presence of organic SEI
453 components in all the deposits. The Li 1s and O 1s signal near LiOH binding energy of all the
454 electrodes potentially imply the presence of LiOH. However, no clear crystalline LiOH is observed
455 in cryo-TEM results (Supplementary Fig. 23). Given the complexity of oxygen's chemical states
456 and local probe of cryoEM, further systematic investigations on the different inorganic species are
457 highly recommended. The weak N 1s spectra of electrodes with DG-based electrolyte suggest trace
458 lithium nitride species. The weak signal around 710 eV in Supplementary Fig. 30 is ascribed to
459 the intrinsic shake structure satellites associated with F 1s (main) and the extrinsic scattered
460 electron background³⁰.

461 The NMR characterization of the electrolyte samples was performed at 25 °C using a Bruker
462 AVANCE III HD spectrometer operating at ¹H frequency of 800 MHz equipped with a 5 mm TCI

463 CryoProbe (Bruker Biospin). The chemical shifts were normalized to tetramethylsilane (TMS).
464 The data were analyzed with Bruker Topspin 4.2.0 with an academic license.

465 After the experiments, the cell was disassembled in the glovebox, and all the dried GDE electrodes
466 after wash treatments can be punched directly into the 3 mm diameter grid in the glovebox
467 (Supplementary Fig. 49), which fits the cryo-TEM holder. All the following steps are consistent
468 with the preparation method shown in the literature using cryo-EM¹⁹. Specifically, each grid was
469 sealed in an individual Teflon-sealed glass vial and wrapping with parafilm. The vial was then
470 transferred from the glovebox and quickly plunged in liquid nitrogen to freeze. Bolt cutters were
471 used to open the vial and tweezers were used to transfer the grid into a cryo-grid box for storages,
472 all under liquid nitrogen. Then, the cryo-grid box with grid under liquid nitrogen was transferred
473 to a cryo-transfer station, and grid was picked up and affixed to the Gatan 626 cryo-transfer holder.
474 The built-in shutter of the transfer holder remained closed as the sample was inserted into the TEM
475 column around 1 second, ensuring that the sample did not come into contact with the air. The cryo-
476 transfer holder maintains the grid at -175 °C during the imaging. Cryo-TEM was conducted on
477 Tecnai T20 G2, and imaging was done with a TVIPS XF416 CCD camera. Electron flux is less
478 than 10 and 300 e Å⁻² s⁻¹ for low-magnification (SADE) and HR-TEM images, respectively. The
479 electron beam exposure time of each area is less than 10 s with acquisition time of 0.4 to 1 s.

480 Calculation methods

481 Density functional theory (DFT) settings: All DFT are performed within the generalized Kohn-
482 Sham scheme³¹, using in the Vienna *Ab initio* Simulation Package (VASP)³², as implemented in
483 Atomic Simulation Environment (ASE)³³. We use the PBE exchange-correlation functional³⁴
484 together with Grimme's D3³⁵ for dispersion corrections, i.e., PBE-D3. Projector augmented wave
485 (PAW) potentials^{36,37} are used with a plane-wave cutoff of 400 eV. The spacing between k points³⁸
486 is chosen as 0.24 Å⁻¹. The Li 1s²2s¹, B 2s²2p¹, O 2s²2p⁴, C 2s²2p², F 2s²2p⁵, and H 1s² electrons
487 are treated explicitly as valence. The electronic energy and structure relaxation were converged
488 within 10⁻⁷ eV and ± 10⁻³ eV Å⁻¹, respectively.

489 All AIMD (Born-Oppenheimer) are performed in the *NVT* ensemble at 300 K. The equations of
490 motion were integrated with a time step of 1 fs using the Nosé-Hoover thermostat^{39,40}. The 100 ps
491 trajectory after the equilibration of the LiBF₄ solvated THF systems is collected for analysis and
492 the 20 ps trajectory after the equilibration of the pure THF solvent system is collected for analysis.
493 All the MD trajectories are converged, with the maximum variance of potential energy within 7
494 meV/atm, marking proper equilibration of the system.

495 The system preparation: For the THF solvent, the supercell of 8.9 Å × 15.4 Å × 14.6 Å is built and
496 contains 16 THF molecules to be equivalent to the THF density of 884.6 Kg m⁻³ at the ambient
497 conditions. 1 LiBF₄ molecule is added in the THF solvent to be equivalent to 0.5 M LiBF₄ in the
498 solvent systems.

500 Data availability

501 All data are available in this article and its Supplementary Information. Source data are provided
502 with this work.

- 503
504 30. Brundle, C.R., Crist, B.V. & Bagus, P.S. Accuracy limitations for composition analysis by
505 XPS using relative peak intensities: LiF as an example. *J. Vac. Sci. Technol. A* **39**, 013202
506 (2020).

- 507 31. Kohn, W. & Sham, L.J. Self-consistent equations including exchange and correlation
508 effects. *Phys. Rev.* **140**, A1133-A1138 (1965).
- 509 32. Kresse, G. & Furthmüller, J. Efficient iterative schemes for ab initio total-energy
510 calculations using a plane-wave basis set. *Phys. Rev. B* **54**, 11169-11186 (1996).
- 511 33. Bahn, S.R. & Jacobsen, K.W. An object-oriented scripting interface to a legacy electronic
512 structure code. *Comput. Sci. Eng.* **4**, 56-66 (2002).
- 513 34. Perdew, J.P., Burke, K. & Ernzerhof, M. Generalized gradient approximation made
514 simple. *Phys. Rev. Lett.* **78**, 1396-1396 (1997).
- 515 35. Grimme, S., Antony, J., Ehrlich, S. & Krieg, H. A consistent and accurate ab initio
516 parametrization of density functional dispersion correction (DFT-D) for the 94 elements
517 H-Pu. *J. Chem. Phys.* **132**, 154104 (2010).
- 518 36. Blöchl, P.E. Projector augmented-wave method. *Phys. Rev. B* **50**, 17953-17979 (1994).
- 519 37. Kresse, G. & Joubert, D. From ultrasoft pseudopotentials to the projector augmented-
520 wave method. *Phys. Rev. B* **59**, 1758-1775 (1999).
- 521 38. Monkhorst, H.J. & Pack, J.D. Special points for Brillouin-zone integrations. *Phys. Rev. B*
522 **13**, 5188-5192 (1976).
- 523 39. Nosé, S. A unified formulation of the constant temperature molecular dynamics methods.
524 *J. Chem. Phys.* **81**, 511-519 (1984).
- 525 40. Hoover, W.G. Canonical dynamics: equilibrium phase-space distributions. *Phys. Rev. A*
526 **31**, 1695-1697 (1985).
- 527

528 Acknowledgments

529 We thank Mathias Ribergaard Vinther and floor managers Brian P. Knudsen, Jakob Ejler Sørensen
530 for helping with the connection of laboratory gas lines, and the build of the mass spectrometer for
531 isotope studies. We thank the NMR center of DTU. We gratefully acknowledge the funding by
532 Villum Fonden, part of the Villum Center for the Science of Sustainable Fuels and Chemicals (V-
533 SUSTAIN grant 9455), Innovationsfonden (E-ammonia grant 9067-00010B), European Research
534 Council (ERC) under the European Union's Horizon 2020 research and innovation programme
535 (grant agreement No 741860), Danish National Research Foundation (VISION DNRF146) and
536 MSCA European Postdoctoral Fellowships (Electro-Ammonia Project 101059643). We thank
537 Xueyan Sun for her assistance to the schematic diagram.

538

539 Author contributions

540 S.L., Y.Z., J.N. and I.C. conceived the paper. S.L. conducted the electrochemical experiments,
541 collected and analysed SEM and XPS data. Y.Z. performed the theoretical calculation. X.F.
542 contribute to the IC measurements and electrochemical experiments. J.B.P. and S.L. did the
543 operando mass spectrometry experiments. M.S. carried out XRD measurements. K.E.R. did the
544 NMR measurement. P.K., C.D.D. and S.L. conducted the cryo-TEM experiments and data
545 analysis. S.Z.A., A.X., R.S., J.B.V.M., N.H.D., J.K. and P.C.K.V. contributed to the data analysis
546 and discussion. S.L. Y.Z. J.N. and I.C. co-wrote the manuscript. All authors discussed the results
547 and assisted during manuscript preparation.

548

549 Competing interests

550 Patent application titled “Flow cell for electrochemical ammonia synthesis” was submitted on
551 09-09-2022 (application number: EP22194879) regarding the reported diglyme solvent in the
552 paper. Inventors: M.S., J.B.P., X.F., S.Z.A., R.S., S.L., Y.Z., K.L., J.K., P.C.K.V., J.K.N., I.C.
553 J.B.V.M, N.H.D. Institution: DTU. The authors except M.S. and S.Z.A., declare no financial
554 conflicts. M.S. and S.Z.A. declare the following competing interests: they have equity ownership
555 in NitroVolt ApS, a Danish company working on commercializing electrochemical ammonia
556 synthesis.

557

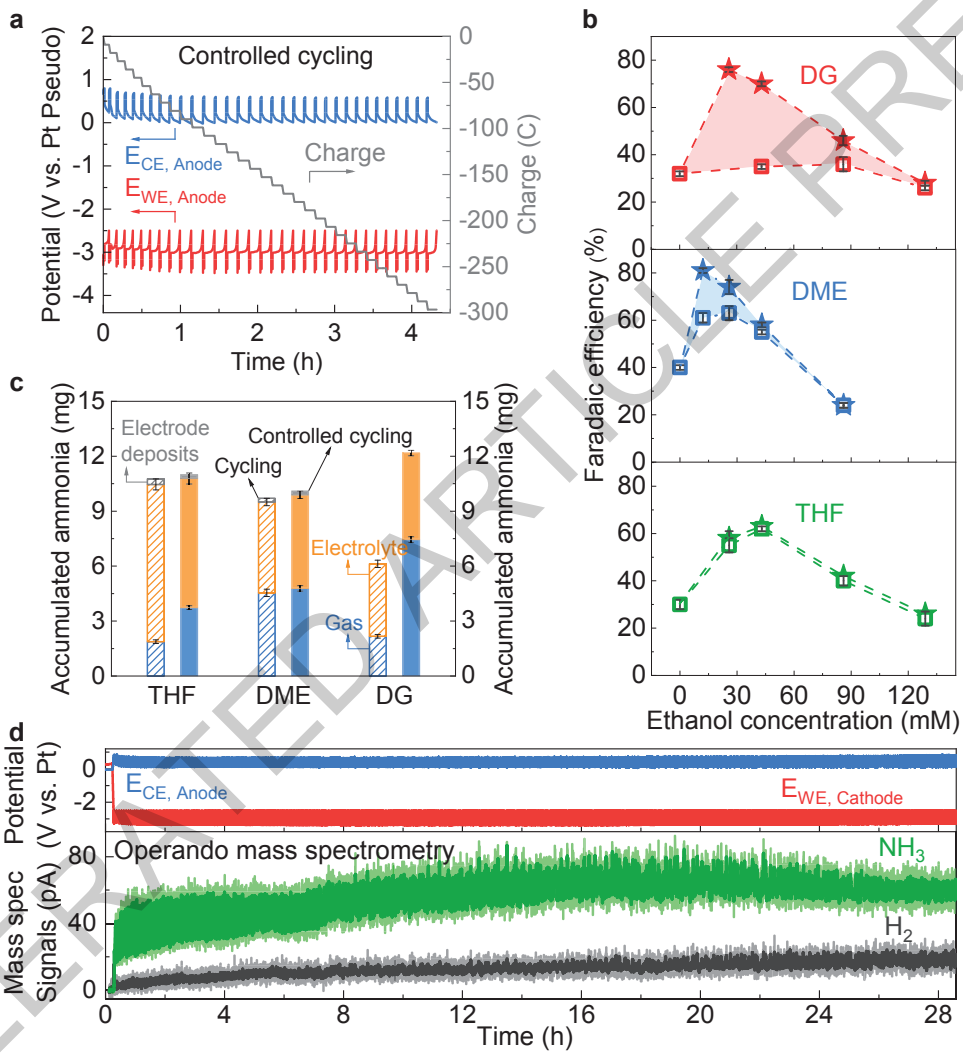
558 **Additional information**

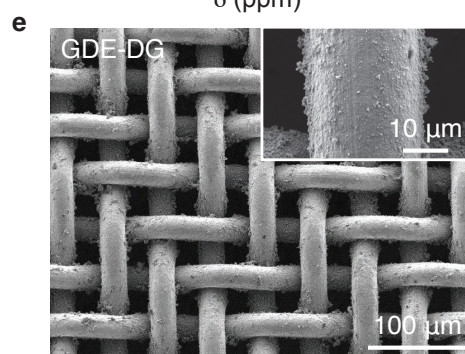
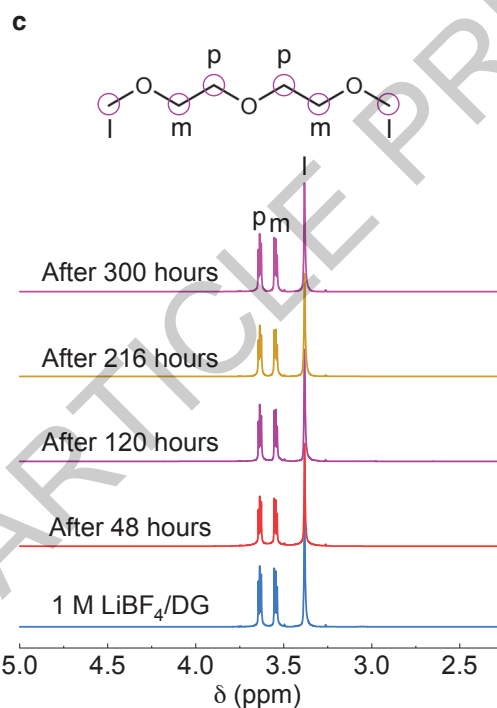
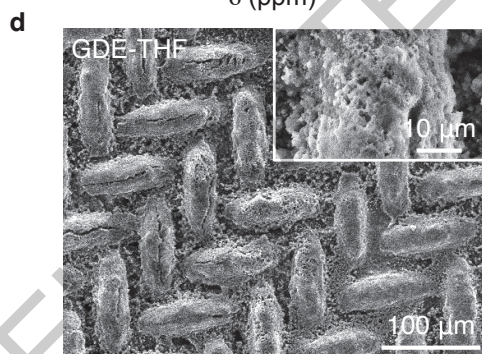
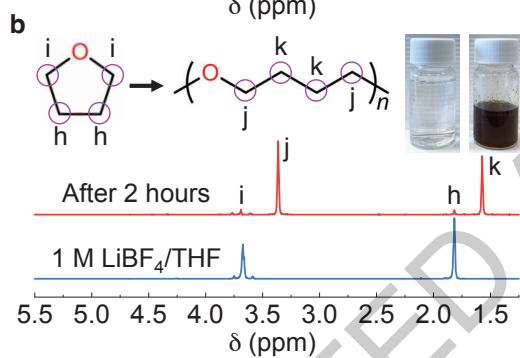
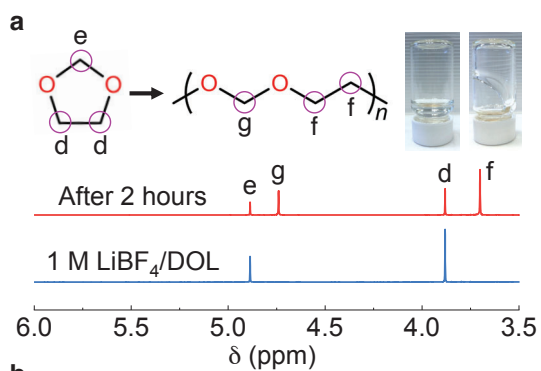
559 **Supplementary Information** is available for this paper.

560 **Correspondence and requests for materials** should be addressed to Ib Chorkendorff.

561 **Peer review information** Nature thanks anonymous reviewers for their contribution to the peer
562 review of this work.

563 **Reprints and permissions information** is available at www.nature.com/reprints.





ACCEPTED MANUSCRIPT

